Sweeping plane dependence of the percolation-induced colossal anisotropic magnetoresistance in spatially confined manganite films

J. Jeon,[1,2,*] J. Jung,[1] and K. H. Chow[1]
[1]*Department of Physics, University of Alberta, Edmonton, AB, Canada T6G 2E1*
[2]*Max Planck Institute for Microstructure Physics, Weinberg 2, 06120 Halle (Saale), Germany*

(Received 11 June 2018; revised manuscript received 12 October 2018; published 29 October 2018)

The angular dependence of the colossal magnetoresistance as the magnetic field is swept in different planes is investigated in a tensile strained La-Pr-Ca-Mn-O microbridge. For the in-plane sweep, the rotation of the magnetic field drives percolation/depercolation of electron conduction channels and in the spatially confined system produces abrupt resistance jumps. As the magnetic field is swept out of the plane of the film towards the direction normal to the film's plane, the relative volume fraction of the ferromagnetic phase is reduced. This leads to depercolation of the conduction channels. This process is reversible when the magnetic field is swept back into the plane of the film.

DOI: 10.1103/PhysRevB.98.144441

I. INTRODUCTION

The existence of unusually large anisotropic magnetoresistance (AMR), i.e., the change in the resistance depending on the direction of the external magnetic field with respect to either the current direction or the crystal axes, in manganite films is of considerable interest due to the possibilities of utilizing these effects in data storage devices [1–4]. Although the exact underlying mechanism of the AMR in manganites remains under investigation, it is widely accepted that the coexistence of competing electronic phases, originating from complex interactions among spin, charge, orbital, and lattice [5,6], plays a prominent role for producing the large AMR [as well as the colossal magnetoresistance (CMR)] [3,4,7].

In many studies, nano/atomic-scale based models are used to explain the origin of the large AMR in manganite films. For example, Fuhr *et al.* have introduced a model based on the electronic structure of manganites plus the spin-orbit coupling to explain AMR in manganite ($La_{0.75}Sr_{0.25}MnO_3$) films deposited on (001) $SrTiO_3$ substrates [4]. Li *et al.* and Dong *et al.* suggested that the anisotropic Jahn-Teller distortion and anisotropic double exchange drive highly anisotropic resistivities and giant AMR near the metal to insulator phase transition temperature of strained manganites [3,8].

Recent experimental studies in manganite films with widths of a few micrometers suggest that relatively large scale (up to few micrometres) electronic phase separation phenomena in certain compositions can also dominate the transport properties, including the AMR and CMR. The $(La_{1-y}Pr_y)_{1-x}Ca_xMnO$ (LPCMO) film (with $x \approx 0.33$ and $y \approx 0.5$) is a well known system that possesses such large size electronic phase (EP) domains [9–12]. In the LPCMO system, it is experimentally shown that the A-site disorder (chemical disorder between La^{3+}-Pr^{3+} and Ca^{2+}) plays a key role in enlarging the size of EP domains [12,13]. This unconventionally large size of EP domains allows LPCMO films with widths of a few μm to "trap" a small number of EP domains within the film [14–16]. As a consequence, changes in the configuration of these domains dominate the transport properties of the entire film and produces interesting transport phenomena that are not observed in bulk materials [16]. For example, one prominent feature is the existence of abrupt resistance jumps when the temperature of the film is changed; these features occur when adjacent metallic domains join or disjoin within the narrow width of the LPCMO film [14,17]. In addition to the resistance jumps, the EP domains within narrow LPCMO films can be arranged such that the system produces interesting multifunctional transport properties such as tunneling magnetoresistance and resistive switching that is not seen in bulk materials [15,16].

In such spatially confined LPCMO films, the ferromagnetic domains change their shape/formation/configuration depending on the direction of external magnetic field to reduce the energy of the system, etc. [18], producing interesting AMR behaviors. For example, Chen *et al.* have reported that "giant" AMR can occur in a manganite stripe (1.6 μm width) due to the elongation of the ferromagnetic metallic (FMM) domains along the direction of the external magnetic field [19]. For instance, when the external magnetic field is applied along the stripe, the elongation of FMM domains creates a conduction path throughout the stripe, whereas the field applied perpendicular to the stripe induces FMM domains to elongate perpendicular to the current direction resulting in disconnected conduction paths throughout the stripe. Alagoz *et al.* have shown that abrupt resistance jumps, which is caused by open/close of the percolation channels, occur in 2 μm width $La_{0.3}Pr_{0.4}Ca_{0.3}MnO_3$ film as the direction of the external field rotates in the plane of the sample [20]. However, the large resistance jumps that are a signature of spatial confinement [14,21] appears to be suppressed in these studies which might reduce the size of the observable AMR (~40%). In our previous studies we reported the fabrication of spatially confined manganite films that exhibit extremely large resistance

*jaechun1@ualberta.ca

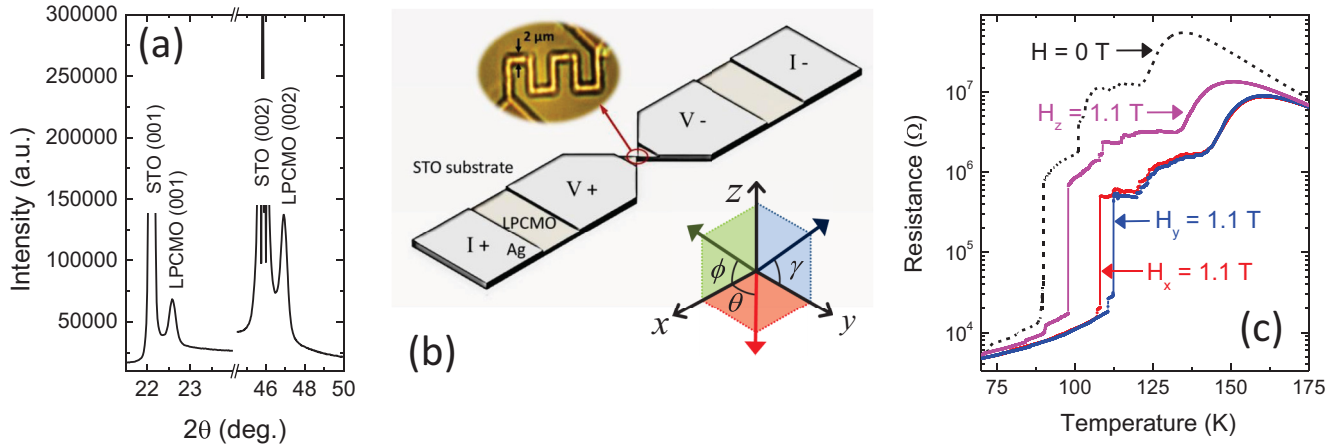

FIG. 1. (a) Results of x-ray diffraction measurements on the sample. (b) An illustration of the measurement geometry; (top-left inset) an optical microscopy image of the sample. (c) The temperature dependence of the resistance at different external field (1.1 T) orientations; H_x, H_y, and H_z denote the field orientation along x, y, and z axis, respectively [see (b)].

jumps in the temperature vs resistance measurements and as a result, "colossal" AMR (C-AMR) effects (up to ∼24 000%) [22,23]. In these reports we suggested that such C-AMR is due to the tendency of FMM domain elongation along a certain orientation upon cooling the system which could originate from the crystallography of the substrate and/or the trapping/pinning of domains via nonuniform distribution of oxygen within the system [12,22]. However, a detailed study of the dependence of the C-AMR effect on the orientation of the sweeping plane of the magnetic field, information that is relevant for applications, is not presently available.

In this paper we present the behavior of the resistance as the external magnetic field rotates in-plane and out-of-plane in a tensile strained La-Pr-Ca-Mn-O microbridge at fixed temperatures. A large resistance drop is found upon the first in-plane angular sweep of the field while relatively small resistance jumps occur in the following sweeps. Interestingly, the large resistance drop is recoverable in a narrow temperature window which leads to the C-AMR effect. By contrast, for the out-of-plane angular sweeps, a recoverable C-AMR effect is found over a wide temperature window. These experimental observations are discussed within the context of the depercolation/percolation of electron conduction channels via changes in the relative volume fraction of ferromagnetic phase as the direction of the magnetic field changes.

II. EXPERIMENTAL METHOD

In this study, a 45-nm-thick $La_{0.3}Pr_{0.4}Ca_{0.3}MnO_3$ (LPCMO) film was first deposited on a $SrTiO_3$ (STO) substrate by using off-axis dc magnetron sputtering (operated at 50 W). The sputtering was carried out at 750 °C in an Ar (20 mTorr)-O_2 (100 mTorr) mixture filled chamber. After the deposition, the sample was cooled to 650 °C and post-annealed at this temperature for 3 h in an oxygen filled chamber near atmospheric pressure. The deposited film was then patterned (2 μm width and 56 μm length with zigzag shape) by using conventional UV lithography and chemical wet etching ($HCl + KI + H_2O$ solution). The x-ray diffraction (XRD) measurement, as shown in Fig. 1(a), was carried out on the prepared sample and confirmed that the film is epitaxial, single phased, and subjected to tensile strain ($\varepsilon_z \approx -1.05\%$). The quality of the pattern was inspected by optical microscope [inset of Fig. 1(b)] and atomic force microscopy (AFM) and confirmed no noticeable physical defects on the sample. For the transport measurements, the Ag electrodes were deposited by on-axis rf magnetron sputtering and indium tipped wires were pressed on the electrodes. The transport properties of the sample were characterized using the standard four point probe method. The measurement setup consisted of a Keithley 2182 current source and Keithley 6221 nanovoltmeter that were controlled using home-built LabView drivers. The angular dependence of the resistance on the external magnetic field was carried out using an electromagnet (GMW 3472-70) with a rotation rate of 1°/s. The geometry of the measurement is illustrated in Fig. 1(b).

III. RESULTS AND DISCUSSION

Examples of the temperature dependencies of the resistance $R(T)$ that were obtained upon cooling the 2 μm width LPCMO film from 300 to 10 K are shown in Fig. 1(c). One of the curves shown was obtained in 0 T while the other three were measured in a field of 1.1 T that was oriented along either the x, y, or z direction. Note the existence of the sharp and abrupt resistance jumps, a signature that sample is in the spatially confined regime. In the LPCMO system, it is known that the electric resistance of the system is dominated by the percolation network throughout the system [9]. The ferromagnetic metallic (FMM) domains, where the conducting electrons mainly travel through, grow and expand the percolation network upon cooling, producing a decrease in the resistance [9,11]. In a narrow (few μm width) LPCMO film, where the conduction network is geometrically limited and hence only a few ferromagnetic domains exists, one can observe a sharp drop of the resistance when a new electron conduction channel is created throughout the sample, i.e., percolation. At a fixed temperature, application of an external magnetic field also results in the growth in the FMM domains, resulting in a reduction in the size of the sharp resistance jump(s) which occurs at a higher temperature compared to the zero field situation [see Fig. 1(c)] [17]. It is noteworthy that the primary resistance

jumps, i.e., the largest resistance jumps, occur at different temperatures depending on the orientation of the magnetic field. For example, the resistance jumps occur at ∼108 and ∼112 K for H_x (field applied along the x axis) and H_y (field applied along the y axis), respectively. Since the AMR is calculated from the difference of the resistances at two different field orientations, this temperature shift, in the temperature range where large resistance jumps occur, is the primary cause of the the colossal magnitude of the in-plane AMR. Outside the temperature window between 108 and 113 K, where the resistances at the two field orientations are similar, the AMR is relatively small. However, when one of the applied field directions is out-of-plane (H_x vs H_z or H_y vs H_z), colossal AMR occurs over a much wider temperature window due to the large shift of the metal-to-insulator phase transition temperature (T_{MIT}). The tensile strain of the LPCMO film due to the STO substrate [see Fig. 1(a)] favors the magnetic easy axes in the plane of the LPCMO film [24,25]. This lowers the relative volume fraction of ferromagnetic phase when the field is applied along the out-of-plane (magnetic hard axis) of the film. As a result the T_{MIT} shifts towards lower temperature [25].

For further understanding of the colossal anisotropic magnetoresistance effect in the sample, the field angular dependence of the resistance measurements [$R(\theta)$-xy plane, $R(\phi)$-xz plane, and $R(\gamma)$-yz plane) were carried out at different temperatures [see Fig. 1(b) for the geometry of the measurement]. For each measurement, the sample was heated up to 300 K, i.e., well above T_{MIT}, then cooled to the measurement temperature in order to reset the formation of the EP domains [26,27]. Figures 2(a)–2(c) show representative $R(\theta)$ curves when the magnetic field is swept in the x-y plane ($\theta = 0^\circ$ to 180° to 0°). Within the temperature range between 108 and 113 K [Fig. 1(c)], percolation-induced resistance jumps are observed as the angle of the magnetic field changes. From the results, it is obvious that the conventional $\cos^2\theta$ dependence or $\sin^2\theta$ dependence is no longer applicable due to the existence of the resistance jumps [4,20]. From 110 to 112 K, a sharp and large persistent resistance drop occurs upon the initial field angular sweeping [Fig. 2(b)]. Here the size of the persistent resistance drop (∼2800%) is nearly the same as the size of the large resistance jump in $R(T)$ measurement (∼3000%). Therefore, one can conclude that the persistent resistance drop is the manifestation of the main percolation event during the initial field sweeping process. In this temperature regime, once such a dramatic resistance drop occurs, the system tends to stay in the lower resistance (percolated) state as the field sweeping continues, although smaller and recoverable resistance jumps (∼47%) still exist in the following sweeps of the magnetic field, indicating percolation/depercolation events are still important in the sample.

Interestingly, there exists a narrow temperature window (∼113 K) where after the initial large resistance drop, the system recovers its initially high resistance value upon further sweeping of the field. Figure 2(c) shows an example of these recoverable percolation/depercolation-induced large resistance jumps. This temperature corresponds to the upper limit of the temperature range where large resistance jumps occurs in the $R(T)$ measurement, i.e., the onset of the C-AMR effect upon cooling. At this particular temperature,

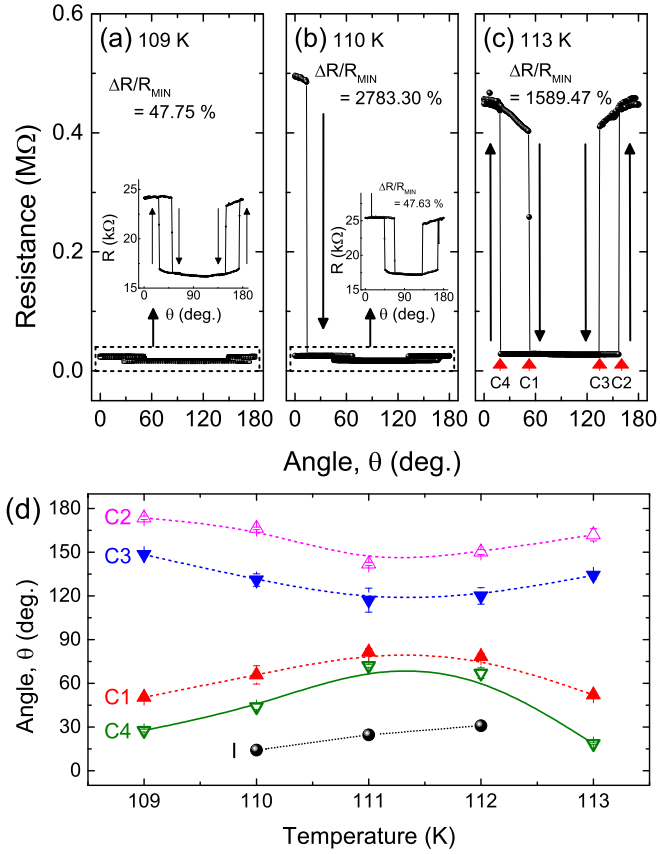

FIG. 2. The angular dependence of the resistance at different temperatures: (a) 109 K, (b) 110 K, and (c) 113 K. (d) The critical angles where the percolation-induced resistance jumps occur at different temperatures.

the field sweeping repeats the creation and destruction of the major conduction path via rearrangement of FMM domains. As a result, recoverable C-AMR (∼1600%) is observed as the sweeping continues. Above this temperature, there is no evidence of any resistance jumps.

Figure 2(d) shows the "critical angles," i.e., where the percolation/depercolation-induced resistance jumps take place, at temperatures between 109 and 113 K. As discussed above, at some temperatures (110–112 K), as θ is first increased from 0°, an initial large drop in the resistance occurs, indicating an initial prominent percolation event within the system. The angle at which this occurs is labeled by I [black dots in Fig. 2(d)]. In the temperature range of 109 to 113 K, regardless of whether this initial event occurs or not, subsequent back and forth sweeps of the magnetic field produces sharp resistance jumps between a low and a high resistance state.

The angles where these jumps take place are labeled by C1, C2, C3, and C4, as illustrated by Fig. 2(c). Namely, as θ is increased from 0°, there exists an angle where the resistance state jumps from a higher to a lower level; this angle is labeled as C1. As θ is further increased towards 180°, a jump from the low resistance level to a higher resistance level takes place at an angle labeled as C2. On the subsequent decrease of θ from 180°, a jump from the high resistance level to a lower resistance level takes place at an angle labeled as C3. Finally, as θ is further decreased, a last jump from the low resistance

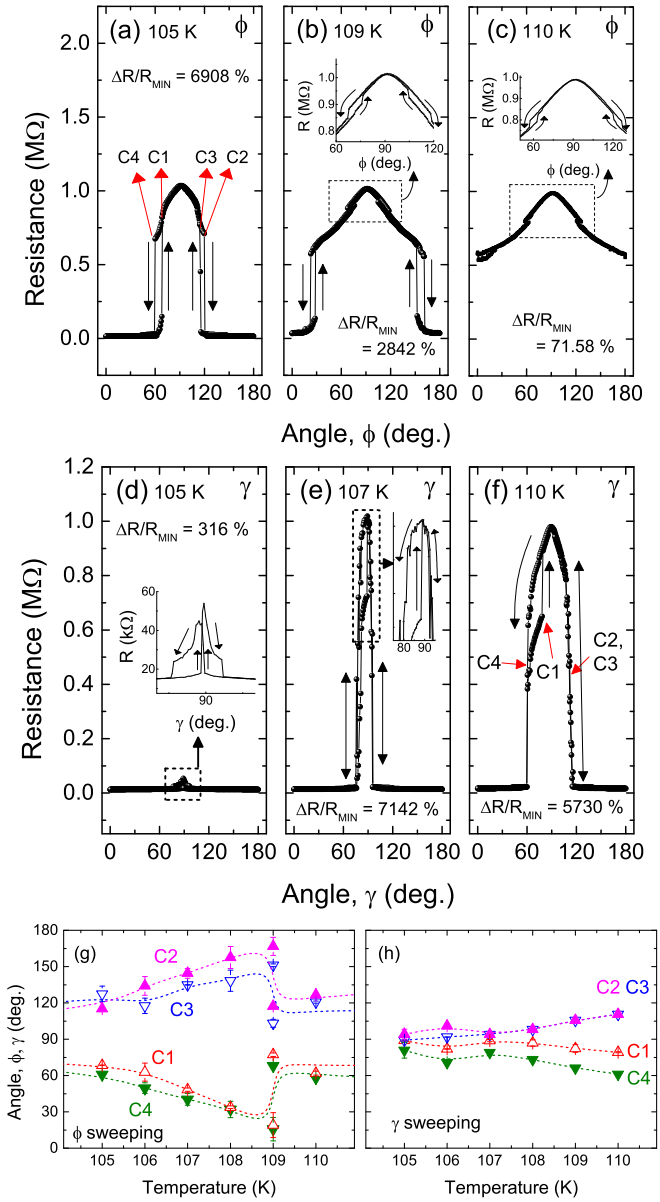

FIG. 3. The angular dependence of the resistance at different temperatures; for the magnetic field swept in the x-z plane (ϕ) (a) 105 K, (b) 109 K, and (c) 110 K; for the magnetic field swept in the y-z plane (γ) (d) 105 K, (e) 107 K, and (f) 110 K. (g) and (h) The critical angles at different temperatures for x-z plane and y-z plane field angular sweepings, respectively.

level to the higher resistance level takes place at an angle labeled as C4.

Figures 3(a)–3(c) and 3(d)–3(f) show angular dependencies of the resistance at different temperatures when the magnetic field is swept in the x-z plane (ϕ) and the y-z plane (γ), respectively. Generally, the resistance is higher when the field is directed out of the plane of the film (the x-y plane), i.e., ϕ or γ not equal to 0° or 180°. Furthermore, it is notable that in the x-z and y-z sweepings, the C-AMR effect (via large resistance jumps; ∼7000% at its maximum) appears over a wider temperature window compared to sweeping in the film's plane (the x-y sweeping).

Recently, Kandpal *et al.* have shown via magnetization measurements on a LPCMO film on STO substrate that the relative volume fraction of the FMM phase is lowered when the field is applied along the magnetic hard axes [25]. This suggests that it is possible for the conduction channel, formed by connection of FMM domains, to disconnect (depercolate) when the field is applied out of the plane of the film. Since the spatially confined system possesses a small number of conduction paths throughout the sample, such a depercolation event can lead to an abrupt resistance jump to a high resistance level. Then, as the field is rotated back to point in the plane of the film, the system "recovers" the FMM volume fraction and the "rejoining" of the adjacent FMM domains leads of a jump of the resistance to a lower level.

Note that the shape of the angular dependence of the resistance is qualitatively different for x-z plane sweeping and y-z plane sweeping. Phenomenologically, this could be due to the tendency of the FMM domains to pin along the y axis of our sample. For in-plane (x-y) sweeping, we have confirmed that the lowest resistance occurs when $\theta = 90°$ (magnetic field along the y axis). Furthermore, the resistance drop occurs at higher temperature for this direction of the magnetic field upon cooling the system in $R(T)$ measurement. This tendency could be caused by preferential domain growth along a certain direction (via domain pinning/trapping) [22,23]. Such preferential domain elongation would play an important role for determining the resistance during the out-of-plane field sweeps. For example, when the field sweeping begins from y axis to z axis, a larger critical angle is needed to depercolate the conduction channel compared to a field sweeping from the x axis to z axis since the FMM domains tend to keep the percolation state along the y axis. The critical angles at different temperatures are shown in Figs. 3(g) and 3(h) for x-z sweeping and y-z sweeping, respectively. Notice that near the verge of the major percolation effect [e.g., ∼109 K for x-z sweeping, Figs. 3(b) and 3(g)], minor percolation events (small resistance jumps) are superimposed on the large resistance jumps. Such percolation events are not observed for y-z sweeping.

In order to quantify the anisotropic magnetoresistance (AMR) of the sample, the temperature dependencies of $\Delta R/R_{\mathrm{MIN}}$ are calculated and compared in Figs. 4(a)–4(c), where ΔR is the difference between the maximum and minimum (R_{MIN}) resistance values in the field angular sweeping measurement at fixed temperatures. In each sweeping plane [(a) x-y plane, (b) x-z plane, and (c) y-z plane), the $\Delta R/R_{\mathrm{MIN}}$ are compared between the values calculated from the $R(T)$ measurement (dotted line), the initial (first) sweep (0° to 180°; closed circles), and the next (second) sweep (0° to 180°; open squares).

As shown in Fig. 4(a), when the magnetic field is swept in-plane (x-y), the first sweep shows AMR values comparable to the AMR calculated from $R(T)$, while the second sweep shows a much smaller magnitude due to the persistent resistance drop during the first angular scan. However, at a temperature that is close to the onset of percolation during cooling (at 113 K), the first and second sweeps show similar C-AMR values [marked with a gray box in Fig. 4(a); also, see Fig. 2(c)]. For the out-of-plane (x-z and y-z plane) sweeps, similar C-AMR values are observed for both the first and the

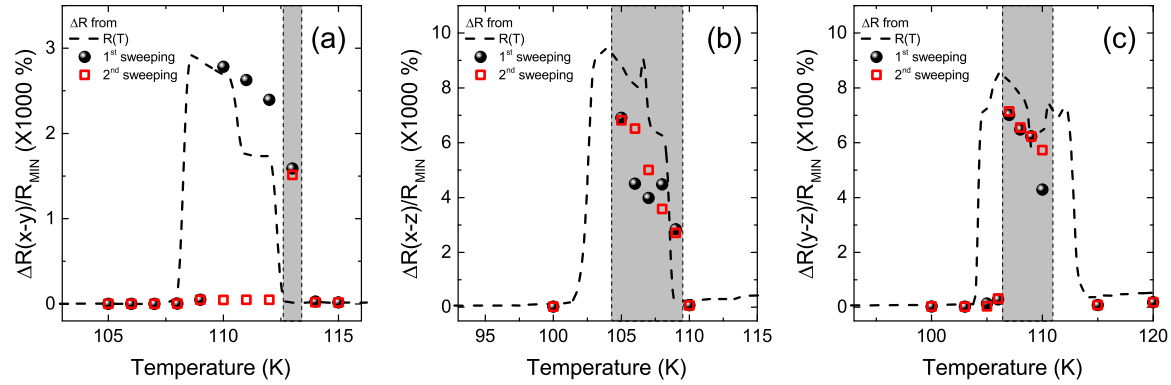

FIG. 4. The comparison of the size of the AMR effect calculated from $R(T)$ measurements (dotted line) and field sweeping at fixed temperatures (closed circles: first sweep, open squares: second sweep) for (a) x-y plane, (b) x-z plane, and (c) y-z plane. The gray box in each plot marks the temperature window where recoverable C-AMR, i.e., where the C-AMR values from the first and second sweeps are similar, occurs.

second sweeps over a wide temperature window [marked with gray boxes in Figs. 4(b) and 4(c)]. It is worth mentioning that the temperature range of the C-AMR corresponds to the sample being in the fluid phase separated state (i.e., FPS state) in which the electronic phase domains are not pinned [28]. In the FPS state, the unpinned electronic phase domains can be effectively manipulated by external perturbations such as electric/magnetic fields which can therefore also rearrange percolation paths through the system [28,29]. Due to the small number of trapped domains in the spatially confined LPCMO films, such changes in the percolation (conduction) path(s) can strongly affect their overall resistance [14,17].

Note that the detailed characteristics of the C-AMR effect (e.g., size and temperature range where it exists) and the critical angles slightly differ with the thermal reset of the sample (heated up to room temperature and cooled down to set temperatures) due to the randomness of phase domain seedings [22,26,27]. Figures 5(a) and 5(b) show the effects of the random nature of the reordered electronic phase domain structure upon thermal reset. Since the largest resistance jump occurs close to the critical temperature and the latter shifts up to few K [see Fig. 5(a) for example], the temperature range where C-AMR exists also changes. Furthermore, even when the temperature is fixed, the resistance jumps that occur during the isothermal rotation of the external magnetic field differ slightly as the rotation continues [see the insets of Fig. 5(b)]. The overall trend, however, is repeatedly observed.

Finally, we would like to point out that the size of the C-AMR is closely related to the size of the largest resistance jump upon cooling the sample. Hence, creating samples with large percolation-induced resistance jumps results in an increased likelihood of these samples having large C-AMR effects. For instance, it may be possible to engineer the size of the percolation-induced resistance jumps and hence the C-AMR effect by artificially creating A-site disorder or modification of the system's oxygen content [12,21].

IV. CONCLUSION

In conclusion, we have investigated the behavior of the colossal anisotropic magnetoresistance in a tensile strained $La_{0.3}Pr_{0.4}Ca_{0.3}MnO_3$ microbridge as the magnetic field is swept in different planes. When the magnetic field is rotated in the plane of the film, it creates/destroys the primary conduction paths via arrangement of the FMM domains. During the out-of-plane sweeping of the magnetic field, the reduction of the relative volume fraction of FMM phase forces the depercolation of the conduction channel as the field approaches the direction normal to the film's plane. The conduction is recovered as the magnetic field direction is reversed towards the plane of the film. We believe that the presented experimental results may provide valuable information for developing novel types of electronic phase domain based electronics.

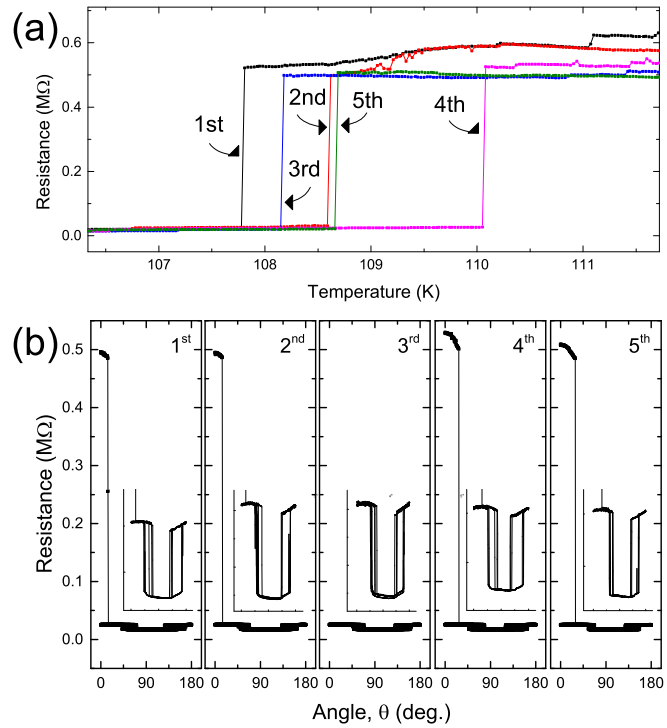

FIG. 5. (a) Field cooled (1.1 T along x axis) $R(T)$ results with thermal resets (heated up to 300 K). (b) Field angular sweeping (x-y plane) results after thermal resets. Note that each field angular dependence of the resistance is measured for three cycles (single cycle = 0° to 180° to 0°). In each run, the critical angles shift slightly.

ACKNOWLEDGMENT

This work was partially supported by the Natural Sciences and Engineering Research Council of Canada.

[1] M. Ziese, Phys. Rev. B **62**, 1044 (2000).
[2] W. Ning, Z. Qu, Y. Zou, L. Ling, L. Zhang, C. Xi, H. Du, R. Li, and Y. Zhang, Appl. Phys. Lett. **98**, 212503 (2011).
[3] R. Li, H. Wang, X. Wang, X. Z. Yu, Y. Matsui, Z. Cheng, B. Shen, E. W. Plummer, and J. Zhang, Proc. Natl. Am. Soc. **106**, 14224 (2009).
[4] J. D. Fuhr, M. Granada, L. B. Steren, and B. Alascio, J. Phys.: Condens. Matter **22**, 146001 (2010).
[5] E. Dagotto, Science **309**, 257 (2005).
[6] E. Dagotto, T. Hotta, and A. Moreo, Phys. Rep. **344**, 1 (2001).
[7] M. Bibes, V. Laukhin, S. Valencia, B. Martínez, J. Fontcuberta, O. Yu. Gorbenko, A. R. Kaul, and J. L. Martínez, J. Phys.: Condens. Matter **17**, 2733 (2005).
[8] S. Dong, S. Yunoki, X. Zhang, C. Sen, J.-M. Liu, and E. Dagotto, Phys. Rev. B **82**, 035118 (2010).
[9] L. Zhang, C. Israel, A. Biswas, R. L. Greene, and A. de Lozanne, Science **298**, 805 (2002).
[10] M. Uehara, S. Mori, C. H. Chen, and S.-W. Cheong, Nature (London) **399**, 560 (1999).
[11] Y. Murakami, H. Kasai, J. J. Kim, S. Mamishin, D. Shindo, S. Mori, and A. Tonomura, Nat. Nanotechnol. **5**, 37 (2010).
[12] Y. Zhu, K. Du, J. Niu, L. Lin, W. Wei, H. Liu, H. Lin, K. Zhang, T. Yang, Y. Kou, J. Shao, X. Gao, X. Xu, X. Wu, S. Dong, L. Yin, and J. Shen, Nat. Commun. **7**, 11260 (2016).
[13] T. Z. Ward, S. Liang, K. Fuchigami, L. F. Yin, E. Dagotto, E. W. Plummer, and J. Shen, Phys. Rev. Lett. **100**, 247204 (2008).
[14] H. Y. Zhai, J. X. Ma, D. T. Gillaspie, X. G. Zhang, T. Z. Ward, E. W. Plummer, and J. Shen, Phys. Rev. Lett. **97**, 167201 (2006).
[15] J. Jeon, J. Jung, and K. Chow, Nanoscale **9**, 19304 (2017).
[16] J. Jeon, J. Jung, and K. Chow, Appl. Phys. Lett. **111**, 242401 (2017).
[17] J. Jeon, H. S. Alagoz, R. Boos, J. Jung, and K. H. Chow, Appl. Phys. Lett. **104**, 122405 (2014).
[18] C. Kittel, Rev. Mod. Phys. **21**, 541 (1949).
[19] J. Chen, W. Wei, K. Zhang, K. Du, Y. Zhu, H. Liu, L. Yin, and J. Shen, Appl. Phys. Lett. **104**, 242405 (2014).
[20] H. S. Alagoz, J. Jeon, R. Boos, R. H. Ahangharnejhad, K. H. Chow, and J. Jung, Appl. Phys. Lett. **105**, 162409 (2014).
[21] J. Jeon. J. Jung, and K. Chow, J. Phys. Soc. Jpn. **86**, 084705 (2017).
[22] J. Jeon, H. S. Alagoz, J. Jung, and K. H. Chow, Appl. Phys. Lett. **107**, 052402 (2015).
[23] J. Jeon, J. Jung, and K. H. Chow, J. Appl. Phys. **120**, 123902 (2016).
[24] J. Dho, Y. N. Kim, Y. S. Hwang, J. C. Kim, and N. H. Hur, Appl. Phys. Lett. **82**, 1434 (2003).
[25] L. M. Kandpal, S. Singh, P. Kumar, P. K. Siwach, A. Gupta, V. P. S. Awana, and H. K. Singh, J. Magn. Magn. Mater. **408**, 60 (2016).
[26] T. Z. Ward, Z. Gai, H. W. Guo, L. F. Yin, and J. Shen, Phys. Rev. B. **83**, 125125 (2011).
[27] T. Z. Ward, X. G. Zhang, L. F. Yin, and X. Q. Zhang, M. Liu, P. C. Snijders, S. Jesse, E. W. Plummer, Z. H. Cheng, E. Dagotto, and J. Shen, Phys. Rev. Lett. **102**, 087201 (2009).
[28] T. Dhakal, J. Tosado, and A. Biswas, Phys. Rev. B **75**, 092404 (2007).
[29] H. Guo, J. H. Noh, S. Dong, P. D. Rack, Z. Gai, X. Xu, E. Dagotto, J. Shen, and T. Z. Ward, Nano Lett. **13**, 3749 (2013).